AAS 26-677

EVENT CAMERA DATASETS FOR LUNAR DESCENT AND PROXIMITY OPERATIONS TRAJECTORIES

Sofia G. Catalan[*], Kyle W. Smith[†], Ronney Lovelace[‡], Davis Adams[§], Trupti Mahendrakar[¶], Cinnamon Wright[‖], Teming Tse[**], Brandon A. Jones[††] and Gavin Mendeck[‡‡]

Event-based cameras offer potential advantages over conventional digital cameras as sensors for a variety of applications. One of the challenges for researchers exploring the use of event cameras as navigation sensors for space environments is collecting high quality datasets due to the cost of access to space. To help address this, we have collected multiple datasets using an event-based camera mounted to a six degree-of-freedom robot over simulated lunar terrain and a scaled docking tunnel model. This paper describes these datasets and details their release into the public domain to enable other researcher teams to develop and test new navigation algorithms.

INTRODUCTION

Event-based cameras have high dynamic range and temporal resolution in comparison with conventional frame cameras, making them potentially powerful sensors for visual odometry in environments with challenging lighting conditions. These environments include the space domain. One of the challenges for researchers exploring the use of event cameras as navigation sensors for space environments is the lack of high quality, relevant datasets due to the cost of access to space. As a result, event camera data is commonly synthetically derived from conventional frame data using software post-processing tools. To help address this, the Safe and Precise Landing: Integrated Capabilities Evolution (SPLICE) project has collected a large amount of data using an event camera mounted to a six degree of freedom robot over both simulated lunar terrain and a scaled docking tunnel model. These datasets include both event camera recordings, frame camera imagery, trajectory files, inertial measurement unit data, a digital elevation map of the terrain model, and a description of the scaled docking target. This data is shared into the public domain in the hope that it will enable researchers to develop and test algorithms for deriving navigation information from event cameras.

[*]Graduate Research Assistant, Department of Aerospace Engineering and Engineering Mechanics, The University of Texas at Austin, 2617 Wichita Street, Austin, TX 78712
[†]Principal Member of Technical Staff, The Charles Stark Draper Laboratory, 17629 El Camino Real, Houston, TX, 77058
[‡]GN&C Engineer, EG-2, NASA JSC, 2101 NASA Parkway, Houston, Texas 77058
[§]GN&C Engineer, EG-2, NASA JSC, 2101 NASA Parkway, Houston, Texas 77058
[¶]GN&C Engineer, Amentum (JETS-II), 2224 Bay Area Boulevard, Houston, Texas 77058
[‖]GN&C Engineer, EG-6, NASA JSC, 2101 NASA Parkway, Houston, Texas 77058
[**]GN&C Engineer, EG-2, NASA JSC, 2101 NASA Parkway, Houston, Texas 77058
[††]Associate Professor, Department of Aerospace Engineering and Engineering Mechanics, The University of Texas at Austin, 2617 Wichita Street, Austin, TX 78712
[‡‡]GN&C Engineer, EG-5, NASA JSC, 2101 NASA Parkway, Houston, Texas 77058

The use of software simulation tools for event cameras has been the primary method of testing downstream algorithms for object detection and navigation in the context of spaceflight. While the costs of the camera hardware have decreased as more commercial applications have conversely increased, sending hardware to space requires significant testing prior to usage as a sensor for operations like rendezvous, proximity operations, and docking, or terrain relative navigation. Interest in event cameras for these spaceflight applications have grown in recent years,[1,2] but the provided datasets have primarily relied on software simulators to emulate the output of event cameras.

Event camera simulators[3,4] rely on sequential image sets with small motion changes (or high time resolution) to compute the differences in each pixel, enabling their tools to provide the pixel-wise change in brightness similar to the response of the real hardware. Additionally, these simulation tools attempt to show a close approximation of the sensor, with functions that emulate pixel activation delays, timing, and noise characteristics. However, the use of input images inherently constrains these simulators to the dynamic range available to the provided frames, i.e. the simulation tools are not able to expand on the brightness sensitivity of the input frames, resulting in an inability to model one of the primary elements that differentiate the event sensors from traditional digital cameras.

CONTRIBUTIONS

In this work, we provide details on a publicly available dataset that aims to enable further research and development for event-based navigation work. With a variety of lighting conditions, trajectories, and target objects, this dataset provides example test cases for both terrain relative navigation and proximity operations.

Data Access

The data presented in this work were collected with the intention of general public release and will ultimately be made available through NASA's TechPort. The data are currently under review. If you are interested in gaining advanced access to this data, please contact the authors directly.

Data Overview

The data is divided into two categories based on the scene they were viewing: Lunar Terrain and Proximity Operations. All tests are described in the provided test_matrix.xlsx file. We also provide calibration data for the two cameras used in our tests.

Lunar Terrain This dataset provides observations of a scaled, 3D printed lunar south pole site with a uniform material. The shadows and observable craters from images taken of this terrain are created by the various lighting conditions that we can set in the lab, i.e. the observed brightness differences are not directly printed on the surface itself. The terrain dataset includes several types of translations and rotations (with variations in velocities) to test different viewing geometries between the cameras and the terrain.

Proximity Operations Using a scaled docking tunnel model, this dataset emulates rendezvous and proximity operations scenarios with our camera setup. Instead of varying trajectories in these tests, the proximity operations dataset focuses on the effect of changing lighting conditions on the observations.

Calibration To enable camera calibration efforts, we include frame images and the raw event stream in our dataset to characterize the cameras' intrinsic and distortion parameters.

TEST ENVIRONMENT

The data presented here was collected in the Simulation, Emulation, Navigation, Sensing, and STAR (SENSS) laboratory* using the Six-DoF Tendon Actuated Robot (STAR) (Figure 1).[5] The SENSS laboratory is an emulation robotics and simulation facility at NASA Johnson Space Center which aids in the rapid development and testing of Spacecraft Guidance, Navigation, and Control systems for applications ranging from rendezvous, proximity operations, docking, precision landing and hazard avoidance, and surface mobility. The SENSS laboratory regularly hosts customers external to Johnson Space Center and supports testing for space-based applications with its own motion, lighting, and target solutions. If interested in learning more about this facility, please contact the authors directly.

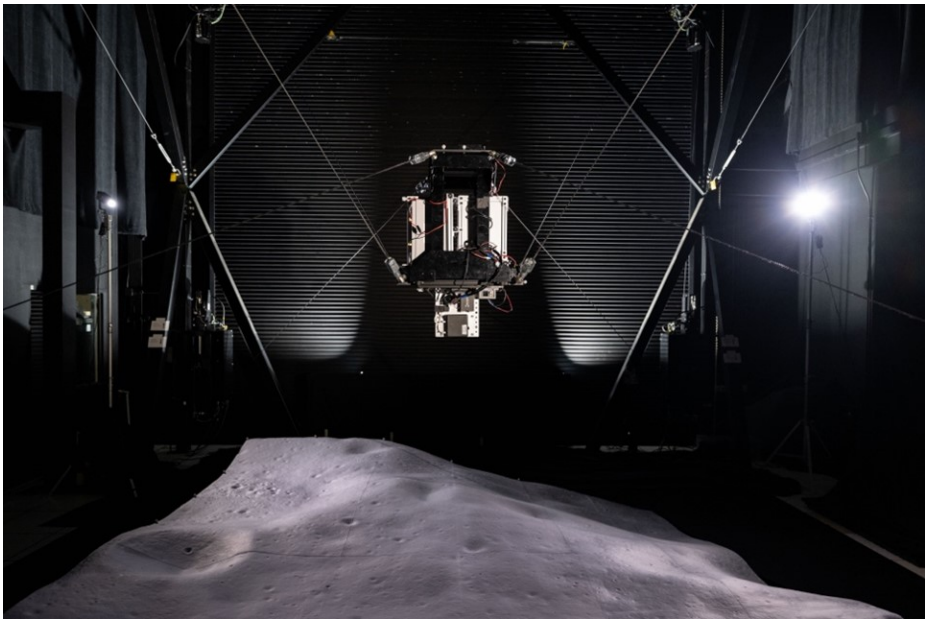


Figure 1: STAR Robot stationed above mock Lunar terrain tiles

Robot

STAR is an omni-directional platform capable of instantaneously moving in all 3 translational and rotational axes. STAR operates within an approximately 5 m spherical operational envelope and is capable of reaching 2 m/s maximum translational velocity, 1m/s^2 translational acceleration, and $\pm 10^\circ$ of rotational motion per axis. The end-effector is capable of supporting a 50 kg payload, including onboard power.

The end-effector is equipped with a 12”x18” aluminum optical plate exhibiting an 1”x1” spaced array of ¼ - 20 mounting holes. Payloads are typically mounted on the bottom of the end-effector to have navigation sensors pointing down. The downward facing payload volume envelope is approximately 20”x20”x30” m (LxWxH).

*A summary for SENSS can be found here: https://ntrs.nasa.gov/citations/20230000141

Coordinate Frames

The STAR and reference frame is displayed in Figure 2. The STAR coordinate frame is centered at the geometric centroid of the robot's mechanical frame. When the end-effector is commanded to move, STAR's encoders will generate a pose estimate of the center of the end-effector based on the current cable lengths for all 8 wenches.

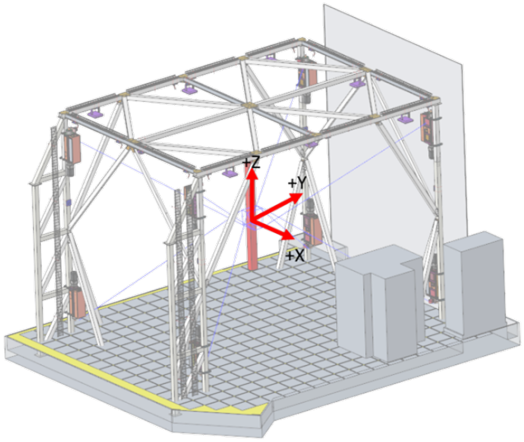


Figure 2: The coordinate frame of the STAR robot used for trajectories

HARDWARE COMPONENTS AND DATA COLLECTION SETUP

Cameras

An event camera and frame camera were mounted next to each other on the STAR end-effector. Both cameras used a Fujinon 35 mm lens (HF15HA-1B) with its aperture set to F/11. A small aperture was chosen to minimize the impact of changing focus as the range from target to camera changes. The same lens was chosen to create similar fields of view, though translational offsets between the cameras cause non-negligible changes in observed scene due to the short ranges from camera to target.

The event-based camera used was a Prophesee EVK4, while the frame camera used was a Teledyne Flir Blackfly S, Mono (BFS-U3-16S2M-CS USB 3.1). Event camera data was logged continuously as single .raw files while frame imagery was recorded at approximately 50 Hz, though the rate is variable. In order to accommodate this high data rate, the imagery was recorded as compressed .jpg. In these tests, we used the default hardware settings for consistency. Future work may consider the inclusion of testing the various bias settings for the data captures, which can help further study the dynamic range response of this sensor.

There was no software-based time synchronization of the data recordings. As an external time synchronization event, the room lights were turned off prior to initializing the robot on its trajectory. This common event is clearly visible in both datasets and can be used to synchronize time. Relative clock drift is likely negligible for applications on the short time scale of the trajectories.

IMU

A VectorNav VN200T IMU was included to provide additional insight into the actual robot end-effector motion. Significant vibration can be observed in the imagery data that is not included in the planned trajectory which are expected deviations from prescribed motion within acceptable limits for the STAR control system. This data was not rigorously time synchronized to the imagery data and may require time biases to be applied to align the IMU outputs to the images by estimating the time of the commanded motion.

Trajectory Files

STAR trajectories are provided as .csv files that are 1000 Hz rates containing time, position, and attitude fields. These describe the state of the end-effector in the STAR coordinate system. The trajectory files do not have a header describing the column fields that correspond to: time (s), x (m), y (m), z (m), roll (deg), pitch (deg), yaw (deg).

The trajectories used for the terrain and proximity operations datasets will be further described in their respective sections below.

LUNAR TERRAIN DATASET

Terrain Model

The SENSS lab houses a set of 3D printed, high-fidelity mock lunar terrain tiles, as displayed in Fig. 1. This set of tiles is an approximately 1:5500 scale of the LM4 Shoemaker Rim C lunar south pole landing site and the elevation data was given in the LOLA dataset.[6] It is important to note that the elevations were not exaggerated from the original data source and are appropriately scaled to the dimensions of the terrain tiles. The terrain was illuminated by a 4x4 array of ORC-TAIKO-2x1 LED light panels. The array was translated around the facility to change the illumination direction and different panels and rows were used to control the incidence angle and light intensity. The light temperature may also be configured, but for our tests they were held constant.

The lighting conditions significantly affect the appearance of the terrain surface due to the elevation changes. Since the surface material color is consistent throughout the surface, the shadow conditions are generated entirely by the light direction and intensity instead of a printed color on the tiles. From the cratered surface and elevation differences, the incidence angle of the light panel can create drastically different observations of the terrain, as shown in Fig. 3.

Lunar Terrain Trajectories and Lighting

26 datasets were collected with the STAR on a simulated descent trajectory over the terrain tiles. Trajectories were generated at variable descent speeds and approach angles relative to the surface, and variations in lighting conditions produced this set of data. Trajectories were collected with either a vertical descent, a horizontal traverse, or a diagonal approach with a 30° glide slope. With respect to the STAR frame, the velocities were varied as 0.1 m/s, 0.4 m/s, or 0.5 m/s. Attitude dynamics included prescribed motion of 0.2°/s within a 5° deadband. The light panel illumination was configured in one of four orientations: low-angle from the south, high-angle from the south, low-angle from the west or high-angle from the west, corresponding orientation of the tiles.

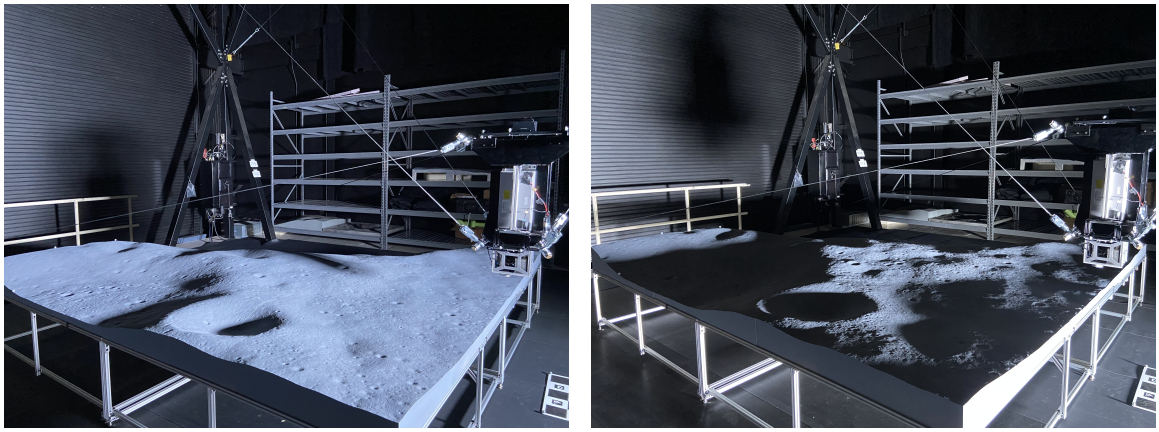


Figure 3: Terrain shadow differences from varied lighting conditions

Terrain Dataset Highlights

Figure 4 provides an example of the observed terrain from the perspective of the frame camera (left) and the event camera (right). While both sensors see the diagonal shadowed area, more texture is clearly visible from the event camera's perspective. The low light capabilities of these event sensors require additional characterization and further distinction between the event and frame cameras may be studied by testing other bias settings on the event camera interface.



Figure 4: Low illumination comparison between an frame image (left) and event image (right)

PROXIMITY OPERATIONS DATASET

Docking Tunnel

Figure 5 shows the docking tunnel model used in the proximity operations dataset. This model was constructed as a scaled version of three main components: the Centerline Docking Target, the Docking Ring, and the Tunnel, with corresponding dimensions shown in Fig. 6.

Centerline Docking Target The specification of the centerline docking target are provided by the International Docking System Standard (IDSS) Interface Definition Document (IDD), Section

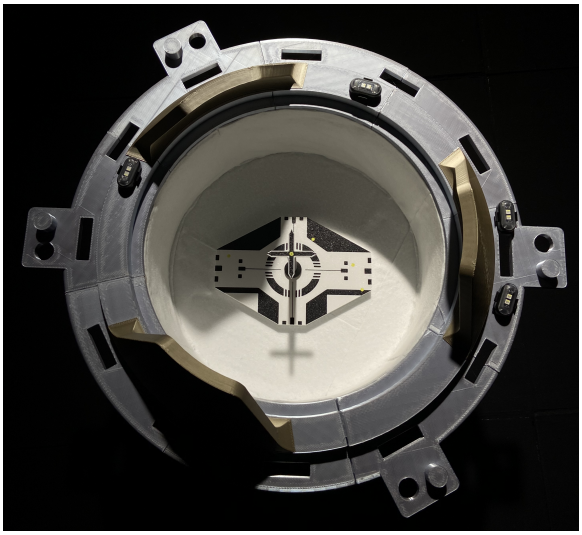


Figure 5: 40% scaled docking tunnel

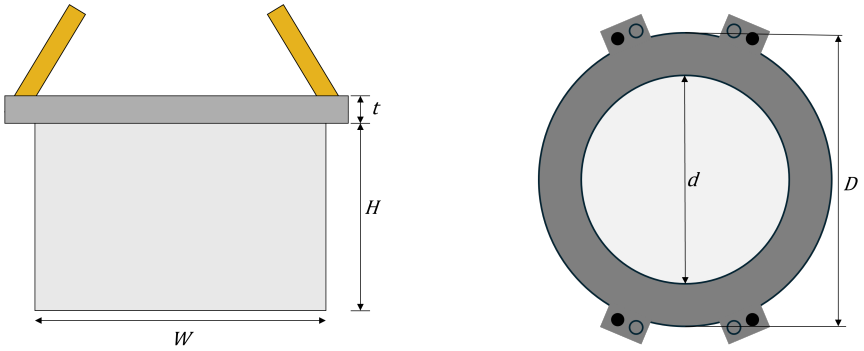


Figure 6: Docking tunnel model drawing

3.5.2.[7] A model based on this specification was developed at approximately 40% scale and 3D printed for testing.

Docking Ring The Docking Ring was based on a publicly available 3D model,[8] represented in the drawing Fig. 6 B. It was scaled so that the total outer diameter is D = 558 mm, the inner diameter is d = 165 mm. The petals shown in Fig. 6 A are attached at the top face of the ring.

LED strobe lights were attached to the docking ring for testing. These lights were placed at deliberately asymmetric locations about the ring and were not surveyed after construction. The strobe lights were only active for a subset of the tests to intentionally stress the dynamic range of the scene.

Tunnel The tunnel was constructed out of foam that molded to fit the base of the ring, shown in drawing Fig. 6 A. The total height of the tunnel without the ring is approximately H = 342.9 mm, measured from the base of the tunnel to the rim (not including the petals). The interior base of the tunnel was also constructed with foam and set at an approximate height of 178 mm above the base of the tunnel. The CDT was set inside the tunnel without highly rigorous positioning or clocking.

The tunnel was illuminated with a Vega Lux 300HP LED Fresnel spotlight at an incidence of approximately 45 degrees. Four Asunder LED Strobe lights were attached to the docking ring and activated for a subset of tests to observe the impact of bright, high frequency lights on frame and event camera data. Additional lighting elements included a flashlight attached to the end effector next to the cameras and a flashlight on the ground, both of which were intended to simulate effects from target and chaser spacecraft.

Proximity Operations Trajectories and Lighting

16 datasets were collected with the STAR on a simulated approach trajectory to the scaled docking tunnel. The proximity operations tests were generated with the same input trajectory for STAR, with an approach velocity of 0.01 m/s. These approaches were done at azimuths of approximately 0, 45, and 90 degrees relative to the orientation of the docking target. A spotlight was used to simulate solar illumination and additional lights included on the STAR end effector and next to the tunnel in order to simulate additional lighting from target or chaser spacecraft. We also included four LED strobe lights on the docking ring that are active in only some of the datasets. The intention of the strobe lights are to provide a high intensity light source that would have potentially detrimental effects on conventional frame imagery, but could be potentially leveraged as an information asset in an event camera data set.

Proximity Operations Dataset Highlights

The proximity operations tests primarily focused on the effects of varied lighting conditions that may be configured to specific rendezvous scenarios. For example, the approaching chaser (with the event camera payload) may bring its own light source, in our case, a flashlight, or the docking target itself may have strobe lights or other light sources that are externally mounted. We emulated other light sources near the field of view to simulate stray light inputs from the sun or reflections from other spacecraft components as well.

In one of our test runs, the STAR-mounted flashlight batteries were depleted and caused an unexpected change in our lighting during the test. Figure 7 shows the frame images (left) and the event images (right) for successive frames (t=0 for image A, B, t=1 for C, D, and t=2 for E, F). At the first time step, the onboard light illuminates the docking target well for both the frame and event cameras. During the abrupt change in lighting when the flashlight powered off, image C shows a completely dark image since the frame camera no longer had the input light source, while image D shows a full field of view activation of events caused by all pixels sensing the light change. In image E, the frame camera's autoexposure is not able to sufficiently adjust to the lower lighting conditions, however, the event camera image F provides a faint observation of the target. This is an example of how the event camera's dynamic range sensitivity may be able to continue providing observations where traditional cameras fail in the low light case.

CALIBRATION DATASET

Typical camera calibration efforts rely on images of a checkerboard taken at varied angles relative to the camera boresight. With these images, OpenCV tools may be used to identify the checkerboard's corners and iteratively compute for the camera intrinsic and distortion parameters. Instead of only relying on moving the target across the field of view, the lighting conditions can also be changed to generate activations in the event camera sensor. To take advantage of this property, the light panel in the SENSS lab was configured to blinkat approximately 5 Hz for the event camera to

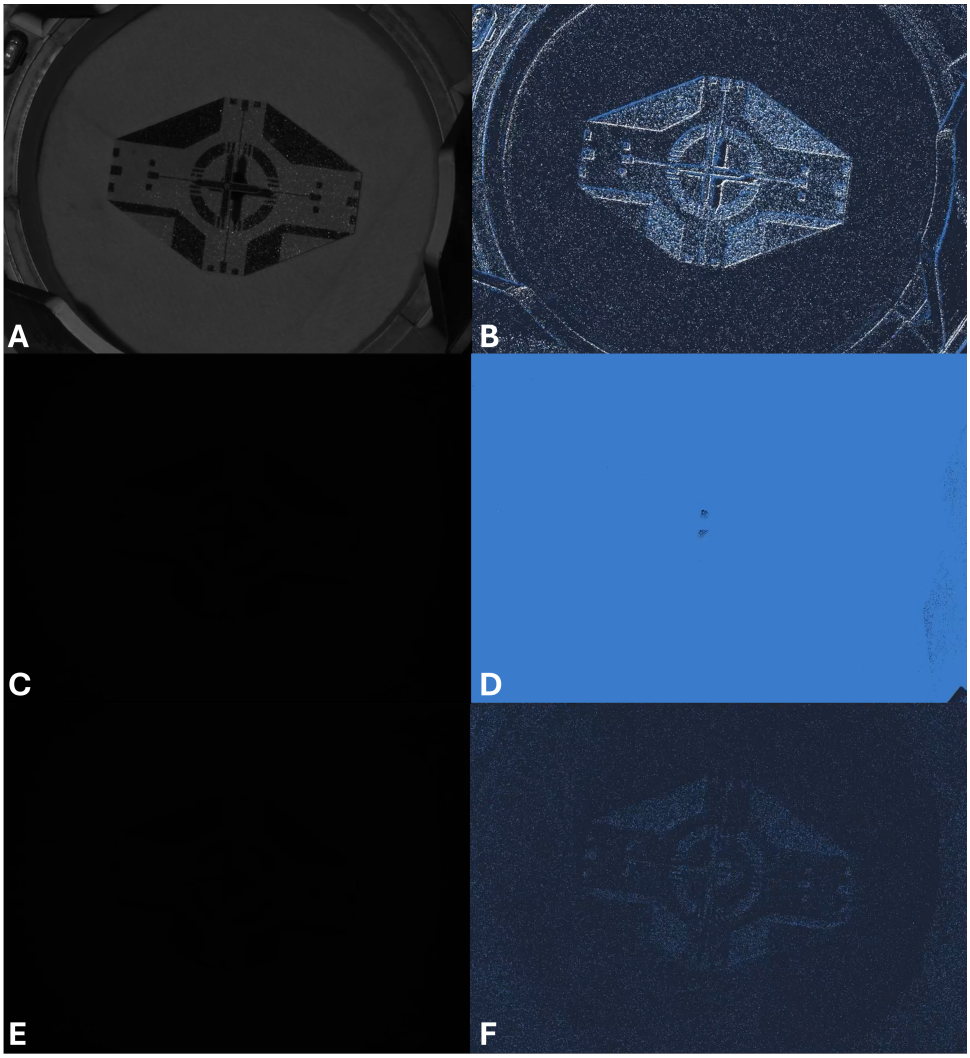


Figure 7: Proximity operations image comparison during a change in lighting conditions

capture the same ChArUco board target as the frame camera used in these tests. Integrating events into an image will then allow the same calibration tools to be used as the frame images, since the board's corners and ArUco markers are observable.

Figure 8 shows the board as observed by the frame and event cameras used in our tests. It is important to note that these cameras do not exactly share a common boresight, but they are mounted next to each other on the STAR end effector.

PRELIMINARY DATA PROCESSING

Following the data collection for the TRN and RPOD scenarios, preliminary work has been started to process the event and frame datasets using tools from the computer vision community. Instead of using methods that directly handle the pixel coordinate activations of the event sensor,[?] our efforts have focused on generating event images by storing sets of events with a user specified integration time. The accumulation of events into images allow us to use methods like visual odom-

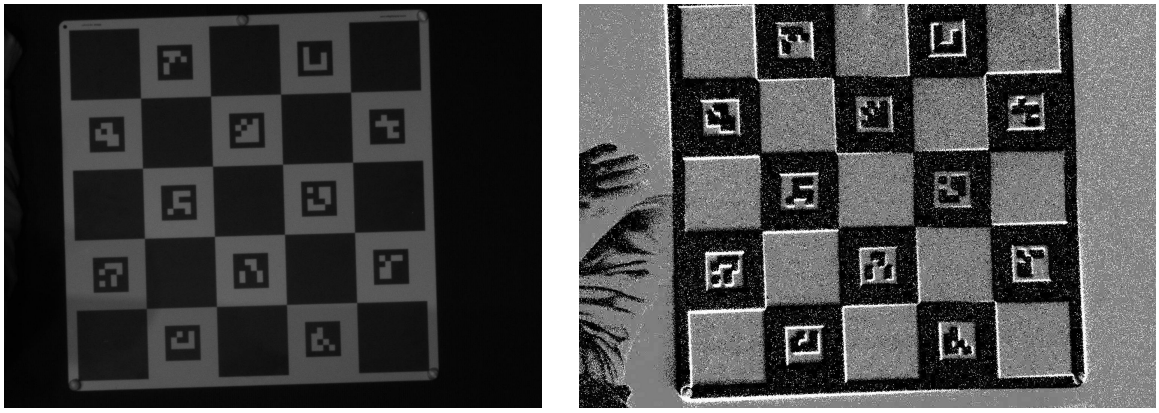


Figure 8: Calibration test images from the frame and event cameras

etry, edge detection, and object tracking that previously have been applied to conventional images. Instead of the RGB channels of regular images, these tools effectively treat the event images as a grayscale input (accounting for the binary positive and negative event activations and the empty background, resulting in 3 distinct pixel values). These methods enable further integration into relative navigation pipelines, but additional work is required to characterize their accuracy in modeling the observed motion and/or change in lighting conditions.

Visual Odometry

Figure 9 provides an example of the visual odometry output from processing event frames, generated with an integration time of 100 ms. With a large enough integration time relative to the velocity in the field of view, common features are visible in successive event images that allow tools like OpenCV to provide estimates of the observable direction and magnitude of motion. In this event image, the motion vectors are plotted on the identified features. With further processing and development, these may be used to provide a velocity-informed measurement to an onboard filter, supplementing frame image-based crater detection and identification methods.

The large gray areas on the bottom half of Fig 10 represent a flat region in the terrain, from which the event camera does not observe any brightness changes. Without observable features, the optical flow method is unable to track motion for the flat area and instead only provides flow vectors from the more textured, cratered regions.

Target Tracking

For an initial characterization of feature extraction from the proximity operations data, the event camera data was converted into convetional frame imagery. A base model of YOLOV11 was tuned to detect the CDT using a combination of real and synthetic imagery.[9] Figure 11 shows the output of an object detection method applied to event images for the centerline docking target. For each event image, the docking target is detected with the provided model confidence value shown on the upper left label of the image. The positive and negative events very clearly show the edges of the external docking ring, the tunnel, and the docking target itself. The center red dot closely corresponds to the target's crosshair in this nadir test and the bounding box consistently tracks the overall target in successive frames.

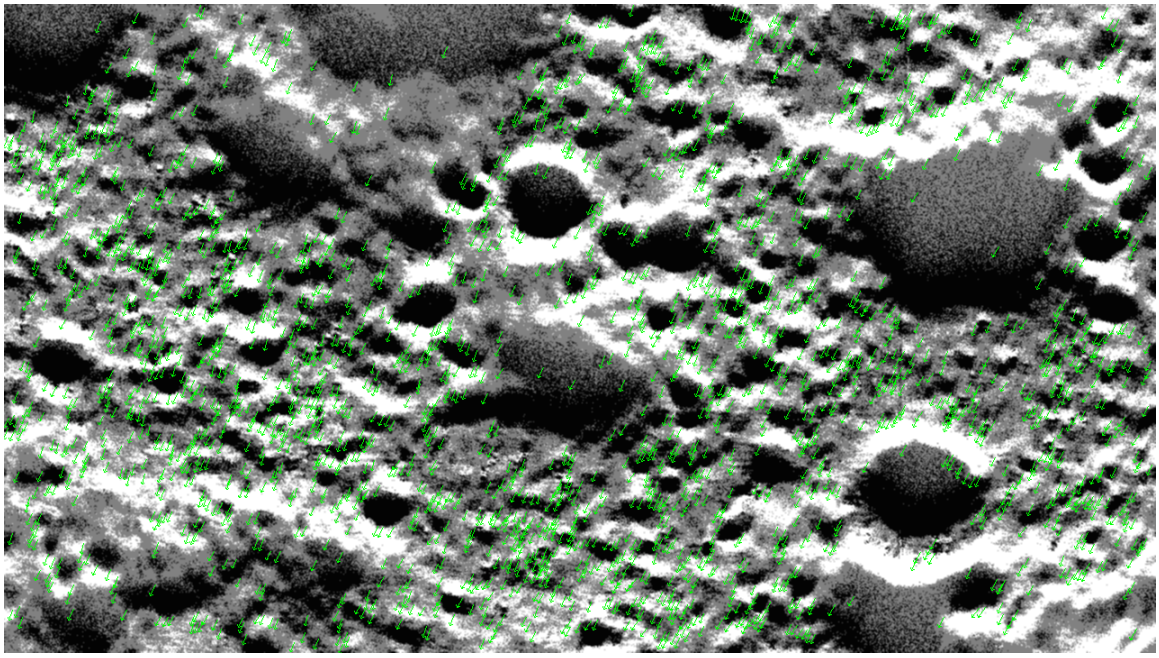


Figure 9: Lucas-Kanade optical flow from observed events of the lunar terrain tiles

DATA COLLECTION CHALLENGES AND FUTURE WORK

Motion Capture Limitations

As a new experimental payload to the SENSS lab, the event camera provided a set of challenges to the data collection process previously used by other work at NASA JSC. The dynamic range sensitivity of these sensors provide an expanded sensing capability, as shown in the examples with difficult lighting conditions in our tests. However, this key feature also prevented us from using the OptiTrack near-infrared motion capture system that accurately tracks the STAR's position because the event data showed an observable, periodic spike in the event count corresponding to the IR flash in preliminary tests. The motion capture system was disabled for the remaining data collection activities to prevent the inclusion of the periodic artifacts in the datasets.

Instead of being able to provide estimates of the robot's true motion throughout the test campaign via an external source, we are limited to providing only the commanded translational and rotational trajectories. However, the inclusion of the IMU data, provided by the VectorNav sensor on the robot enables us to correlate the robot's vibration to the observable event data's motion in frame.

Material Properties and Lighting

In future work, either with further tests in the SENSS lab or in other uses of event cameras, this sensitivity to periodic light flashing may be explored as a known input for data captures. With the expectation that the event count spike, given a periodically flashing light source, the event camera can provide a low cost alternative to other more expensive sensors for observing very quickly changing motion or lighting conditions.

The overall fidelity of our test set up may also be improved in future work. Since the expected change in brightness defines the event sensor's ability to capture data, the material properties and

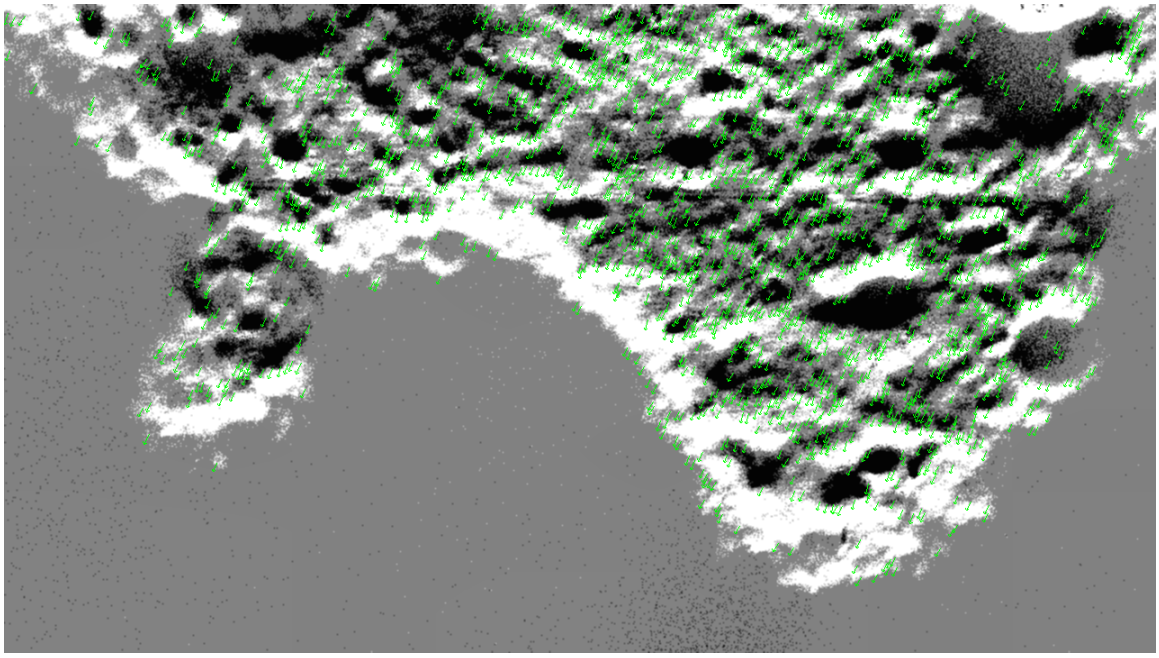


Figure 10: Lucas-Kanade optical flow with flat terrain area

light intensity of the experiment will directly impact the observed events. Here we have relied on 3D printed materials that result in line and texture artifacts that may have observable differences compared to using real spacecraft materials. Previous work[10] has shown how event cameras may be used to distinguish responses from varying materials, which may be used for component identification on spacecraft. Future work may include similar lab tests to further quantify these material-based effects, as a function of lighting direction and intensity, and camera range to the target surface.

Test Procedures Improvements

Safety procedures during tests in the SENSS lab require that personnel actively watch the motion of the robot as it runs through each trajectory. During experiments with low light conditions, it was difficult to visually inspect the robot along with the tensioned cables that enable its motion. For one of these tests, an emergency stop was triggered by the robot itself when one cable's tension was too low. This resulted in a work stoppage for the day while the system was reset. This could have been prevented by an earlier manual command by the operators, if we had better visibility to the robot itself. In future efforts, we may consider using additional room lights or a STAR-mounted light while also using a baffle for the event camera to limit the stray light input to the sensor. The SENSS lab can take advantage of the lessons learned through these event camera experiments, as it further supports other projects and programs by enabling tests with various hardware payloads, targets, lighting conditions, etc.

ACKNOWLEDGEMENTS

This work was partially supported by the NASA Space Technology Graduate Research Opportunities (NSTGRO) Fellowship 80NSSC22K1202.

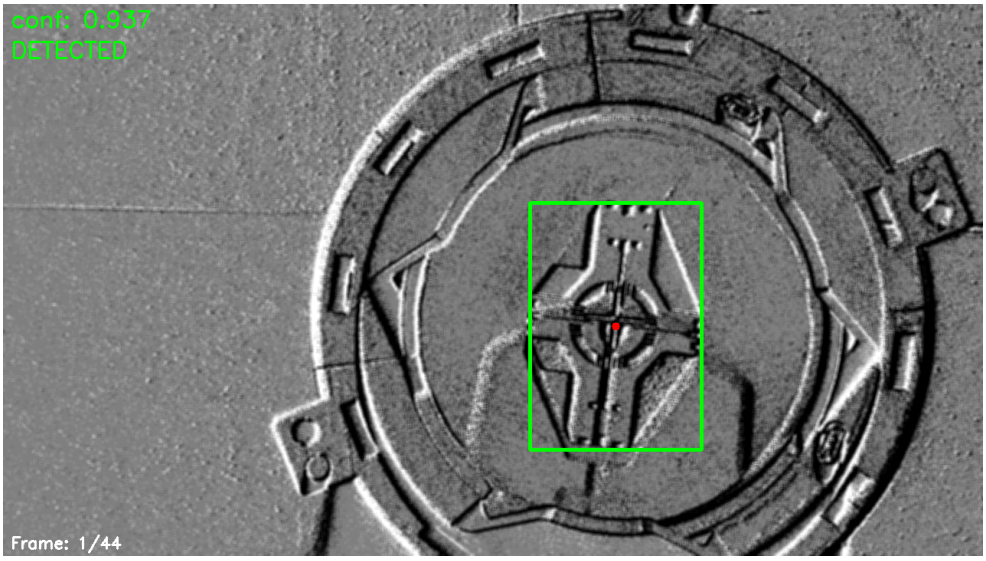


Figure 11: Docking target tracking using event images

CONCLUSIONS

Here we describe a large dataset of event camera, frame camera, and IMU recordings that were collected using robotic trajectories over two relevant spaceflight scenes. This dataset will be available in the public domain at the time of this manuscript's publication. The goal of releasing this dataset is to enable researchers to test and develop navigation algorithms that leverage the full capabilities of event cameras, removing some of the limitations of frame-based synthetic event data.

REFERENCES

[1] L. J. Azzalini, E. Blazquez, A. Hadjiivanov, G. Meoni, and D. Izzo, "On the Generation of a Synthetic Event-Based Vision Dataset for Navigation and Landing," Aug. 2023. arXiv:2308.00394 [cs], 10.48550/arXiv.2308.00394.

[2] L. Azzalini, "Tracking particles ejected from active asteroid Bennu with event-based vision," Dec. 2023, pp. 567–571, 10.21741/9781644902813-124.

[3] D. Joubert, A. Marcireau, N. Ralph, A. Jolley, A. Van Schaik, and G. Cohen, "Event Camera Simulator Improvements via Characterized Parameters," *Front. Neurosci.*, Vol. 15, July 2021, p. 702765, 10.3389/fnins.2021.702765.

[4] Y. Hu, S.-C. Liu, and T. Delbruck, "v2e: From Video Frames to Realistic DVS Events,"

[5] D. W. Adams, T. Tse, S. Downs, R. R. Sostaric, J. Sooknanan, D. Bankieris, S. O'Meara, C. Peck, M. Majji, H. L. Sanchez, *et al.*, "Entry, Descent, and Landing GN&C System Evaluation via Cable-Driven Emulation Robotics," *AIAA SCITECH 2023 Forum*, 2023, p. 2325.

[6] M. K. Barker, E. Mazarico, G. A. Neumann, D. E. Smith, M. T. Zuber, and J. W. Head, "Improved LOLA elevation maps for south pole landing sites: Error estimates and their impact on illumination conditions," *Planetary and Space Science*, Vol. 203, 2021, p. 105119.

[7] S. R. Donahoe, "International Docking System Standard (IDSS) Interface Definition Document (IDD) Revision F," tech. rep., 2022.

[8] dreava, "Artistic NASA Standard Docking System," `https://www.thingiverse.com/thing:3078712`, Sept. 2018. Thingiverse model, accessed March 18, 2026.

[9] G. Jocher and J. Qiu, "Ultralytics YOLO11," 2024.

[10] A. Jolley, G. Cohen, D. Joubert, and A. Lambert, "Evaluation of event-based sensors for satellite material characterization," *Journal of Spacecraft and Rockets*, Vol. 59, No. 2, 2022, pp. 627–636.